DESL · EPFL

# PMU-based situational awareness systems for the monitoring, protection and control of active distribution networks

**Prof. Mario Paolone**
**EPFL Distributed Electrical Systems Laboratory (EPFL-DESL)**

# Context and motivations

# Motivations

## Planned introduction of wide area monitoring systems for **power transmission networks [1]**

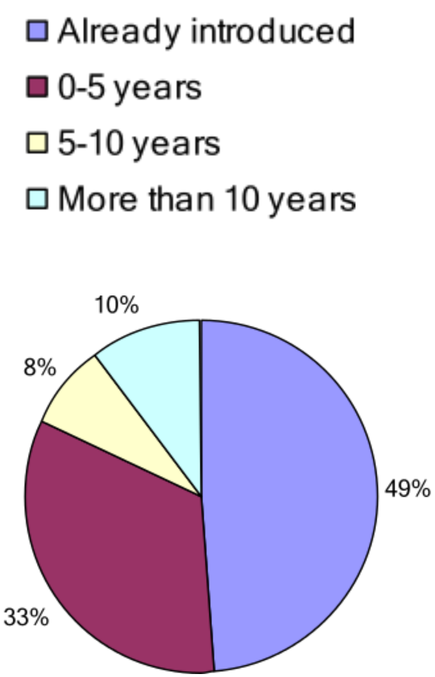


## Benefits power transmission networks [2]

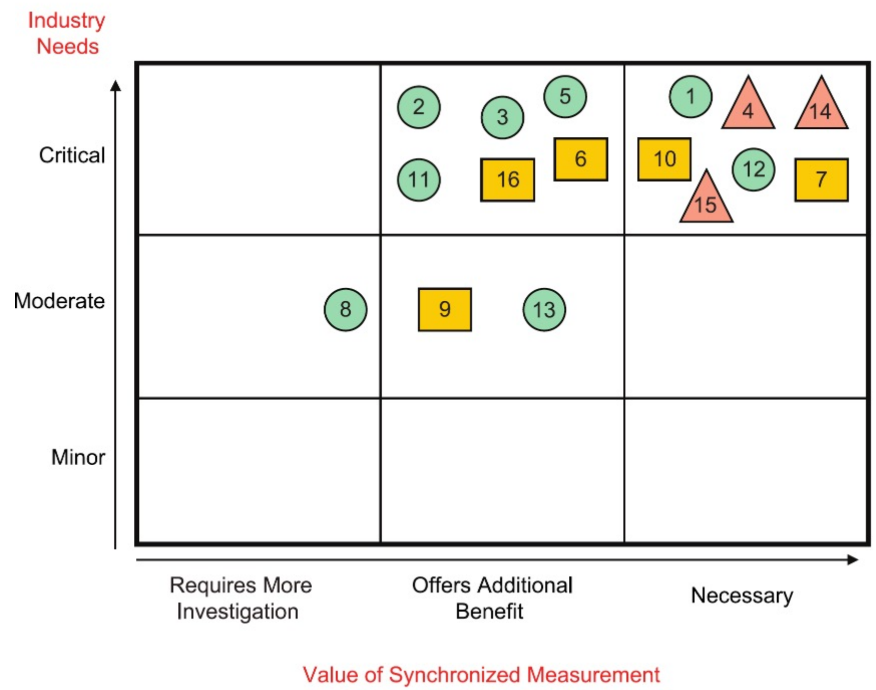


| | |
|---|---|
| 1 | Angle/Freq. monitoring |
| 2 | Voltage stability monitoring |
| 3 | Thermal overload monitoring |
| 4 | Real-time control |
| 5 | State estimation (improvement) |
| 6 | State estimation (boundary) |
| 7 | State measurement (linear) |
| 8 | WA stabilization |
| 9 | Adaptive protection |
| 10 | Congestion management |
| 11 | Power-system restoration |
| 12 | Post-mortem analysis |
| 13 | Model benchmarking and parameter estimation (steady-state) |
| 14 | Model benchmarking and parameter estimation (dynamic) |
| 15 | Planned power-system separation |
| 16 | DG/IPP applications |

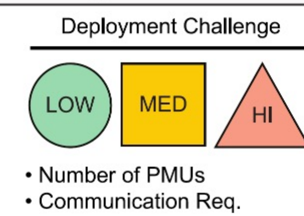

# Motivations

## Benefits power distribution systems

### Monitoring

- Real-time visualization and alarming
- **Real-time state estimation**
- Post-event analysis
- Planning of grid reinfor-cement due to excessive DER penetration
- Asset management
- Equipment misoperation
- System health monitoring

### Protection

- **Fault identification**
- **Fault location**
- Fault isolation

### Control

- Voltage control
- Line congestion management
- Grid-aware control of distributed resources
- Islanding (and back-synchronization to the main grid)
- System restoration

**Requirement: joint P+M class to avoid devices duplication**

# PMU accuracy requirements for distribution systems

# PMU accuracy requirements for the SE in DSs [3]

Compared to transmission networks, power distribution systems are characterized by:

- **Shorter line lengths** (5-10 km max)
- **Lower feeder impedances**
- **Reduced power flows** (typically <10 MVA)

↓

***Small amplitude and phase differences between bus voltage and line current synchrophasors measured in adjacent nodes.***

***Do we really need to measure such small angle differences ?***

Additionally, waveform disturbances are more remarkable:

- **Harmonic distortion** beyond the IEEE Std. C37.118 specs:
  - Superposition of multiple harmonic components (see EN 50160)
  - Harmonics superposed to (potential) inter-harmonics.
- Higher **measurement noise**, particularly in the measured currents.
- **Faster dynamics** related to the RER short-term volatility.

# PMU accuracy requirements for the SE in DSs [3]

Let us consider the use case of **PMU-based state estimation (SE) in distribution systems. Type, placement and accuracy of measurement devices have a significant impact on the state estimation accuracy.** Consequently, a specific sensitivity analysis may be conducted with respect to these characteristics to analyze the SE performance.

**The physical system:** let us consider the simple case of a two-ports equivalent of a generic passive reciprocal branch of a power grid.

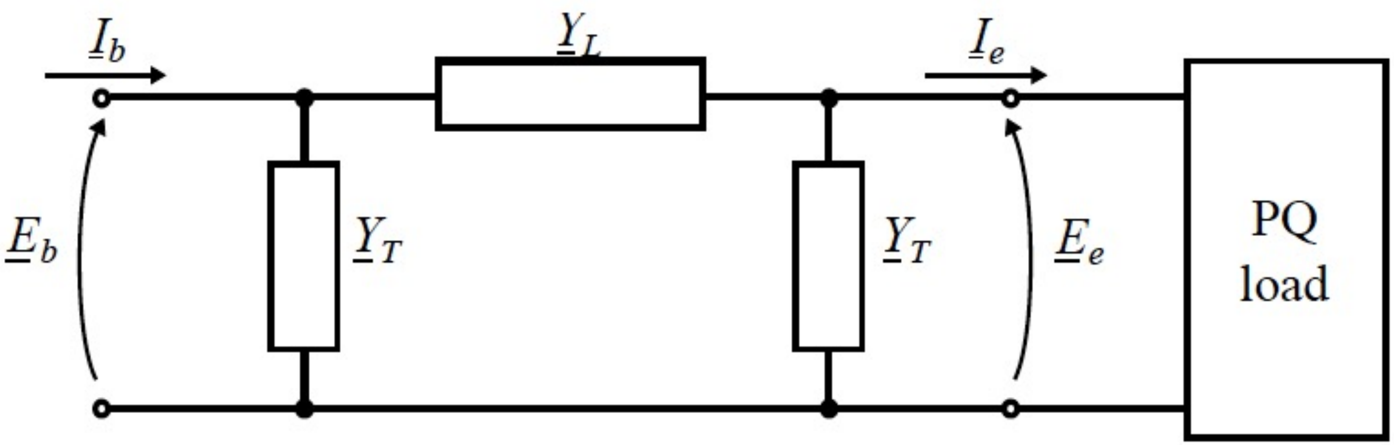


$\underline{Y}_L = [(r + jx) \cdot L]^{-1}$ Branch longitudinal admittance (known)

$\underline{Y}_T = (g + jb) / 2 \cdot L$ Branch shunt admittance (known)

# PMU accuracy requirements for the SE in DSs [3]

**Six possible measurement configurations (with no redundancy):**

a. $(\underline{E}_b^M, \underline{E}_e^M)$ b. $(\underline{I}_b^M, \underline{I}_e^M)$ c. $(\underline{E}_e^M, \underline{I}_e^M)$

d. $(\underline{E}_b^M, \underline{I}_b^M)$ e. $(\underline{E}_e^M, \underline{I}_b^M)$ f. $(\underline{E}_b^M, \underline{I}_e^M)$

Note that, since the two-ports branch equivalent is assumed to be reciprocal, configurations c, d, e and f are interchangeable.

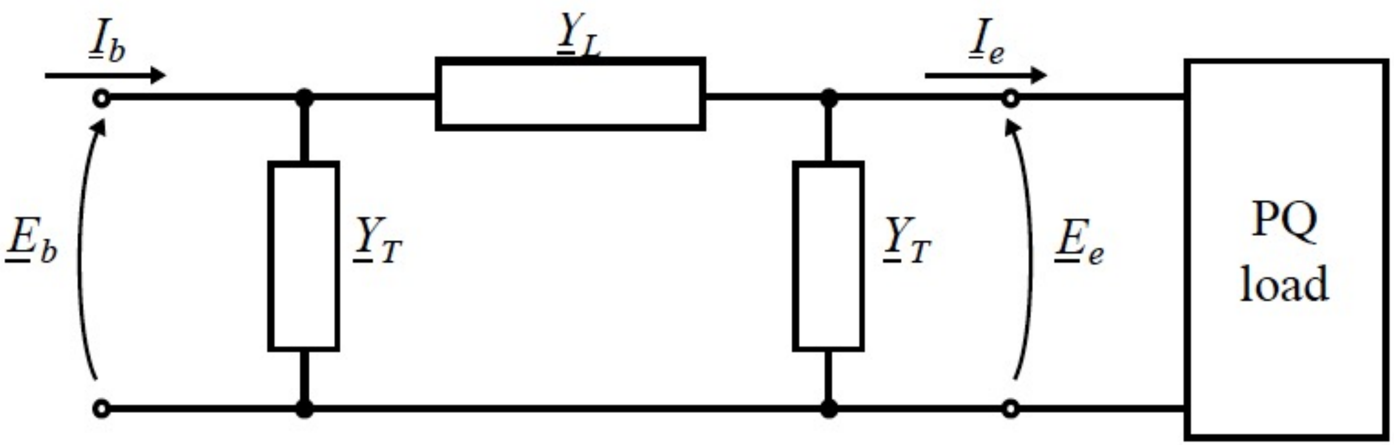

# PMU accuracy requirements for the SE in DSs [3]

The computed quantities (indicated with apex C) are derived by means of the auxiliary matrices that correspond to the three considered measurement configurations (measured quantities indicated with apex M):

$$a.\quad \begin{bmatrix} \underline{I}_b^C \\ \underline{I}_e^C \end{bmatrix} = \begin{bmatrix} \underline{Y}_T + \underline{Y}_L & -\underline{Y}_L \\ \underline{Y}_L & -(\underline{Y}_T + \underline{Y}_L) \end{bmatrix} \begin{bmatrix} \underline{E}_b^M \\ \underline{E}_e^M \end{bmatrix}$$

$$b.\quad \begin{bmatrix} \underline{E}_b^C \\ \underline{E}_e^C \end{bmatrix} = \begin{bmatrix} \dfrac{\underline{Y}_L + \underline{Y}_T}{\underline{Y}_T(2\underline{Y}_L + \underline{Y}_T)} & \dfrac{-\underline{Y}_L}{\underline{Y}_T(2\underline{Y}_L + \underline{Y}_T)} \\ \dfrac{\underline{Y}_L}{\underline{Y}_T(2\underline{Y}_L + \underline{Y}_T)} & \dfrac{-(\underline{Y}_L + \underline{Y}_T)}{\underline{Y}_T(2\underline{Y}_L + \underline{Y}_T)} \end{bmatrix} \begin{bmatrix} \underline{I}_b^M \\ \underline{I}_e^M \end{bmatrix}$$

$$c.\quad \begin{bmatrix} \underline{E}_b^C \\ \underline{I}_b^C \end{bmatrix} = \begin{bmatrix} \dfrac{\underline{Y}_L + \underline{Y}_T}{\underline{Y}_L} & \dfrac{1}{\underline{Y}_L} \\ \underline{Y}_T\left[2 + \dfrac{\underline{Y}_T}{\underline{Y}_L}\right] & \dfrac{\underline{Y}_L + \underline{Y}_T}{\underline{Y}_L} \end{bmatrix} \begin{bmatrix} \underline{E}_e^M \\ \underline{I}_e^M \end{bmatrix}$$

# PMU accuracy requirements for the SE in DSs [3]

**The measurement model: measurements uncertainty and measurement configuration** play a crucial role on the **evaluation of the accuracy of the computed quantities**.

We are interested in **quantifying the influence of the magnitude and phase measurement errors separately**. Therefore, the variation of the magnitude error, assuming a null phase error, allows evaluating the effect of the magnitude error and vice versa.

As known, the performance of a PMU can be expressed in terms of total vector error (TVE). The **maximum magnitude error** $err_m$ (respectively **phase error** $err_p$) is calculated from the assumed TVE by considering a null phase (respectively magnitude) error:

$$err_m = f(TVE)\big|_{err_p=0} \quad , \quad err_p = f(TVE)\big|_{err_m=0}$$

We simulate the measurements by adding to the true values of the measured quantities a randomly-generated noise ($\Delta m$ for the magnitude and $\Delta p$ for the phase) assumed to be **Gaussian, white and with a standard deviation equal to 1/3 of the maximum error in order to cover the 99.7 % of the Gaussian distribution.**

$$\Delta m \quad N(0, err_m / 3) \qquad X_m^M = X_m^T + \Delta m$$

$$\Delta p \quad N(0, err_p / 3) \qquad X_p^M = X_p^T + \Delta p$$

# PMU accuracy requirements for the SE in DSs [3]

## The assessment procedure

1. A power flow is computed by imposing the powers at the end of the line, in order to determine the **true state of the system**.

2. $N$ sets of measurements are obtained by **perturbing the true quantities inferred from step 1 with randomly generated white noise**. The selected number of draws is equal to $10^4$ in order to infer statistical distributions that are numerically significant.

3. $N$ sets of **computed quantities are calculated by applying the auxiliary matrices of Slide #9 to each set of measurements**. Then, we calculate the errors as the difference between computed and true quantities.

4. The accuracy of the computed quantities is represented by the stds of the probability distributions of the errors calculated in step 3.

# PMU accuracy requirements for the SE in DSs [3]

## The numerical example

Parameters of typical overhead lines used in medium-voltage power distribution systems.

| **Line type** | $r$ [Ω/km] | $x$ [Ω/km] | $g$ [μS/km] | $b$ [μS/km] | $L$ [km] |
|---|---|---|---|---|---|
| overhead | 0.268 | 0.346 | 0 | 3.36 | 5 |

Imposed power flows at the end of the line, power factor equal to 0.9 (lagging).

| | | | | |
|---|---|---|---|---|
| $S$ [kVA] | 1 | 10 | 100 | 2000 |

# PMU accuracy requirements for the SE in DSs [3]

## Numerical results

**Measurement config #a.**

$$\begin{bmatrix} \underline{I}_b^C \\ \underline{I}_e^C \end{bmatrix} = \begin{bmatrix} \underline{Y}_T + \underline{Y}_L & -\underline{Y}_L \\ \underline{Y}_L & -(\underline{Y}_T + \underline{Y}_L) \end{bmatrix} \begin{bmatrix} \underline{E}_b^M \\ \underline{E}_e^M \end{bmatrix}$$

**Accuracy of the mag and phase of $\boldsymbol{I_b^C}$**(same results are obtained for $I_e^C$) as a fcn of the uncertainty of the mag and phase of the **voltage measurements** expressed in TVE %.

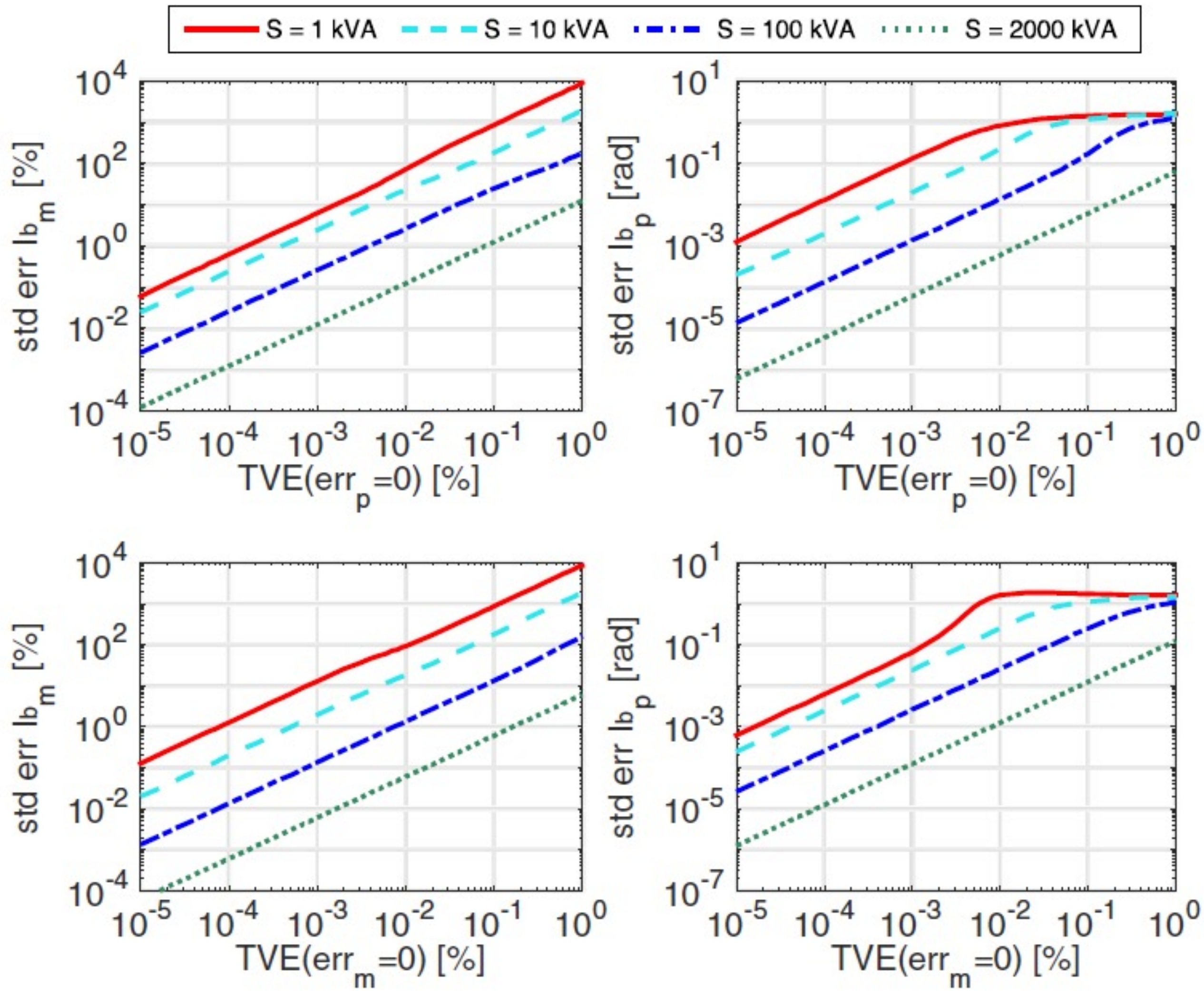


Note that the bottom curves exhibit a knee in the case of high measurement uncertainty. This is due to the fact that the phase error has an upper bound of π radians.

# PMU accuracy requirements for the SE in DSs [3]

## Numerical results

**Measurement config #b.**

$$\begin{bmatrix} \underline{E}_b^C \\ \underline{E}_e^C \end{bmatrix} = \begin{bmatrix} \dfrac{\underline{Y}_L + \underline{Y}_T}{\underline{Y}_T(2\underline{Y}_L + \underline{Y}_T)} & \dfrac{-\underline{Y}_L}{\underline{Y}_T(2\underline{Y}_L + \underline{Y}_T)} \\ \dfrac{\underline{Y}_L}{\underline{Y}_T(2\underline{Y}_L + \underline{Y}_T)} & \dfrac{-(\underline{Y}_L + \underline{Y}_T)}{\underline{Y}_T(2\underline{Y}_L + \underline{Y}_T)} \end{bmatrix} \begin{bmatrix} \underline{I}_b^M \\ \underline{I}_e^M \end{bmatrix}$$

**Accuracy of the mag and phase of $E_b^C$**(same results are obtained for $E_e^C$) as a fcn of the uncertainty of the mag and phase of the **current measurements** expressed in TVE %.

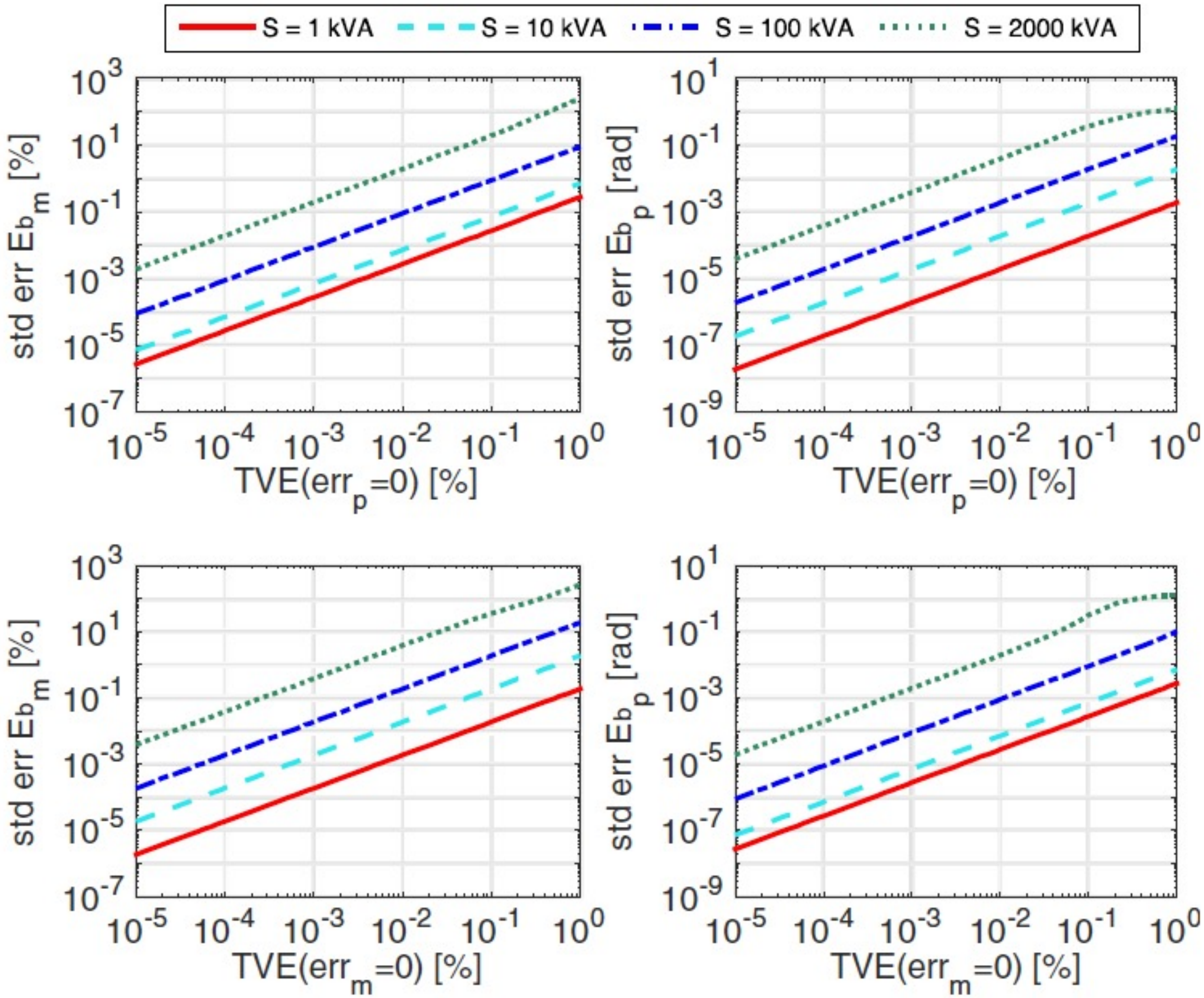


Note that the bottom curves exhibit a knee in the case of high measurement uncertainty. This is due to the fact that the phase error has an upper bound of $\pi$ radians.

# PMU accuracy requirements for the SE in DSs [3]

## Numerical results

**Measurement config #c.**

$$\begin{bmatrix} \underline{E}_b^C \\ \underline{I}_b^C \end{bmatrix} = \begin{bmatrix} \dfrac{\underline{Y}_L + \underline{Y}_T}{\underline{Y}_L} & \dfrac{1}{\underline{Y}_L} \\ \underline{Y}_T \left[ 2 + \dfrac{\underline{Y}_T}{\underline{Y}_L} \right] & \dfrac{\underline{Y}_L + \underline{Y}_T}{\underline{Y}_L} \end{bmatrix} \begin{bmatrix} \underline{E}_e^M \\ \underline{I}_e^M \end{bmatrix}$$

**Upper graphs show the accuracy of the magnitude of $\boldsymbol{E_b^C}$ and $\boldsymbol{I_b^C}$** as a fcn of the uncertainty of the mag of $\boldsymbol{E_e^M}$ and $\boldsymbol{I_e^M}$ expressed in TVE %.

The two bottom graphs refer to the phase of the above-mentioned quantities.

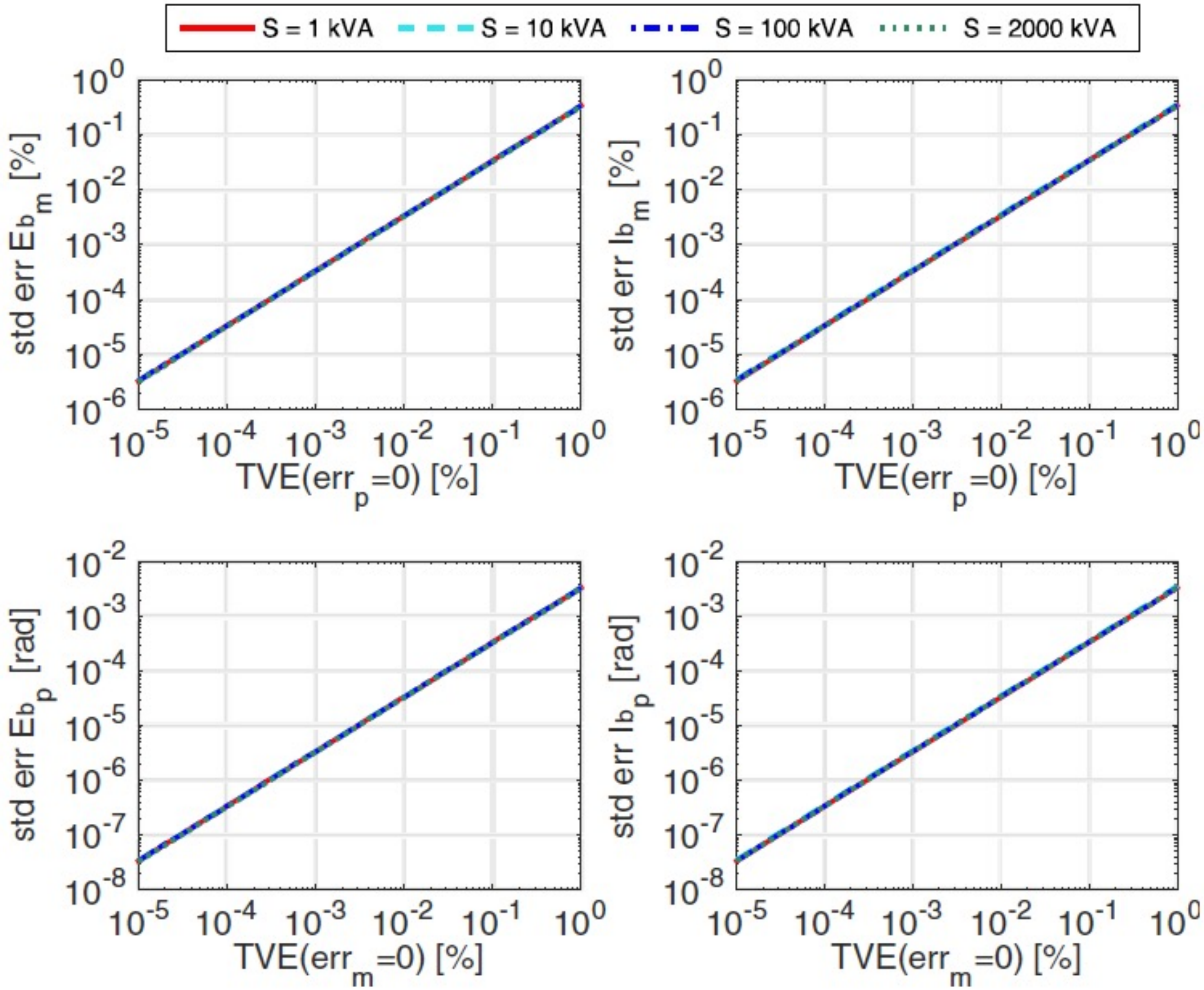

# Extension to complex distribution systems

# Extension to complex distribution systems [3-5]

- **Static SE**: infers the system state by using only current time information (e.g., **Weighted Least Squares – WLS – or Least Absolute Value methods**).

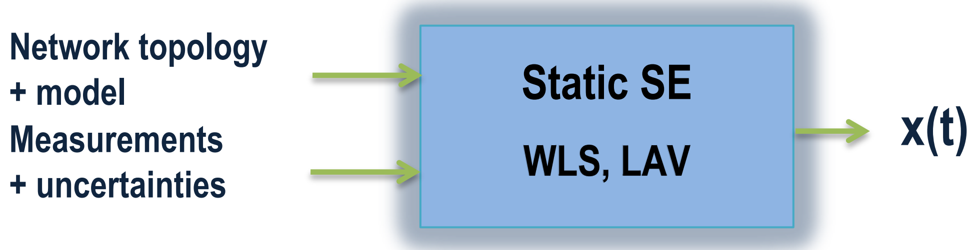


- **Recursive SE**: takes into account information available from previous time steps and predict the state vector in time (e.g., **Kalman Filter – KF – method**).

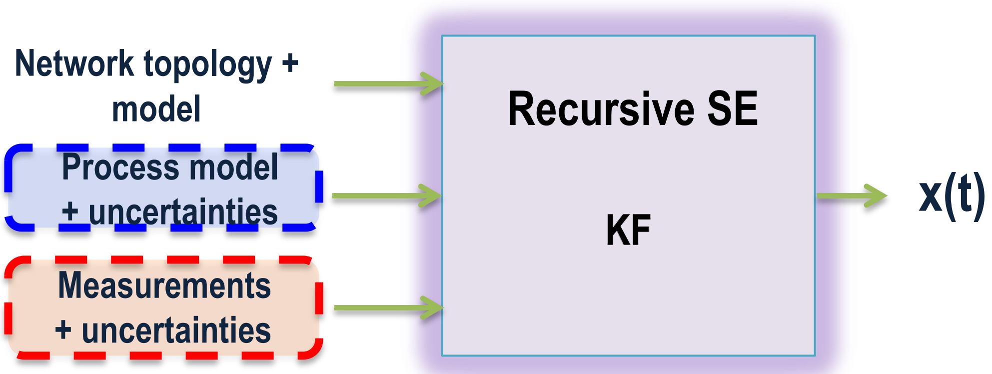


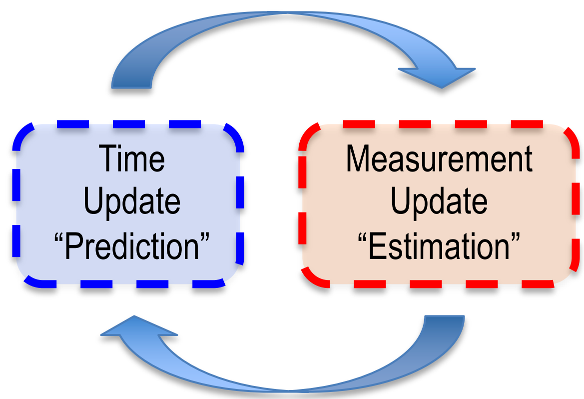

# Discrete Kalman Filter [5]

| Prediction Equations |
|---|
| Prediction of the state: $\tilde{\mathbf{x}}_t = \mathbf{A}\hat{\mathbf{x}}_{t-1} + \mathbf{B}\mathbf{u}_{t-1}$ <br> $\tilde{\mathbf{P}}_t \equiv \mathbf{A}\hat{\mathbf{P}}_{t-1}\mathbf{A}^T + \mathbf{Q}_{t-1}$ |

| Estimation Equations |
|---|
| (1) Computation of the **Kalman Gain**: $\mathbf{K}_t = \tilde{\mathbf{P}}_t\mathbf{H}^T(\mathbf{H}\tilde{\mathbf{P}}_t\mathbf{H}^T + \mathbf{R})^{-1}$ |
| (2) Estimation of the state $\hat{\mathbf{x}}_t = \tilde{\mathbf{x}}_t + \mathbf{K}_t(\mathbf{z}_t - \mathbf{H}\tilde{\mathbf{x}}_t)$ <br> $\hat{\mathbf{P}}_t \equiv (\mathbf{I} - \mathbf{K}_t\mathbf{H})\tilde{\mathbf{P}}_t$ |

- $\mathbf{x}_t$ and $\mathbf{x}_{t-1}$ represent the state of the system in correspondence of time steps $t$ and $t$-1, respectively;
- $\mathbf{u}_{t-1}$ represents a set of $u_c$ control variables (independent from the system state) of the system at time step $t$ -1;
- $\mathbf{w}_{t-1}$ represents the system process noise assumed white and with a normal probability distribution;
- $\mathbf{A}$ is a matrix linking that state of the system at time step $t$-1 with the one of the current time step $t$ for the case of null active injections and process noise;
- $\mathbf{B}$ is a matrix that links the time evolution of the system state with the $u_c$ controls at time step $t$-1 for the case of null process noise;
- $\tilde{\mathbf{P}}_t$ is the prediction error covariance matrix;
- $\mathbf{K}$ is the Kalman gain;
- $\hat{\mathbf{P}}_t$ is the estimation error covariance matrix.

# Discrete Kalman Filter [5]

Since we are targeting power distribution systems, it is worth reminding that the peculiar characteristics of these networks (e.g., high level of imbalance of lines, loads, and Distributed Generators) require the adoption of **3-phase unbalanced** SE process.

Moreover, the adopted Discrete Kalman Filter (DKF)-SE relies only on measurements provided by PMUs that allows for a measurement matrix $\mathbf{H}$ consisting of constant elements, namely: zeros, ones, and elements of the 3-ph network compound admittance matrix.

# Extension to complex distribution systems [3-5]

A DKF state estimator (DKF-SE) accuracy is evaluated for the following measurement configurations:

- ***Conf. A*: voltage phasors in every bus;**
- ***Conf. B*: injected current phasors in the slack-bus and voltage phasors in the other buses;**
- ***Conf. C*: injected current phasors in every bus;**
- ***Conf. D*: voltage phasors in the slack-bus and injected current phasors in the other buses;**
- ***Conf. E*: voltage and injected current phasors in every bus.**

The assessment procedure

1. A power flow is computed by imposing the powers at the nodes of the system, in order to determine the **true state of the network**.
2. $N$ sets of measurements are obtained by **perturbing the true quantities inferred from step 1 with randomly generated Gaussian noise**. The selected number of draws is equal to $10^4$. The maximum errors $err_m$ and $err_p$ refer to the cumulated error of a PMU and a 0.1-class sensor. Assuming the sensor error is predominant yields: $err_m = 0.1\ \%$ and $err_p = 1.5$ mrad. The corresponding TVE is equal to 0.18%;
3. Each set of measurements is then processed by the DKF-SE in order to get $N$ sets of estimated states. We calculate the estimation errors as the difference between estimated and true state
4. The SE accuracy is represented by the means and stds of the probability distributions of the estimation errors calculated in step 3.

# Extension to complex distribution systems [3-5]

## The network

- Modified 3-phase IEEE 13-bus distribution test feeder
- 15 kV rated voltage.
- Untransposed lines corresponding to the configuration #602.
- Bus #650 represents the connection to a sub-transmission network characterized by a short circuit power $S_{sc} = 300$ MVA and a ratio between real and imaginary parts of the short circuit impedance $R_{sc} / X_{sc} = 0.1$. The two lines connecting bus #633 to #634 and #671 to #692 are assumed to be 300 feet long.

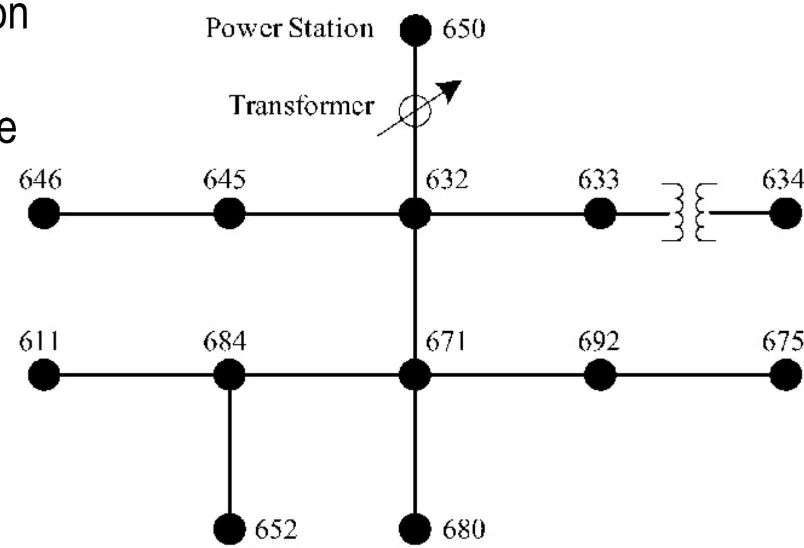


## Loading conditions

- Case 1 (low-load scenario): each load absorbs 10 kVA.
- Case 2 (high-load scenario): each load absorbs 1000 kVA.
- In both cases the power is equally distributed among the three phases and a lag power factor of 0.9 is assumed.

# Extension to complex distribution systems [3-5]

## Numerical results – Case 1 (low load scenario)

Means and stds of the estimation errors of magnitude/phase of voltages and injected currents for each measurement config (only the largest error among the three phases is shown).

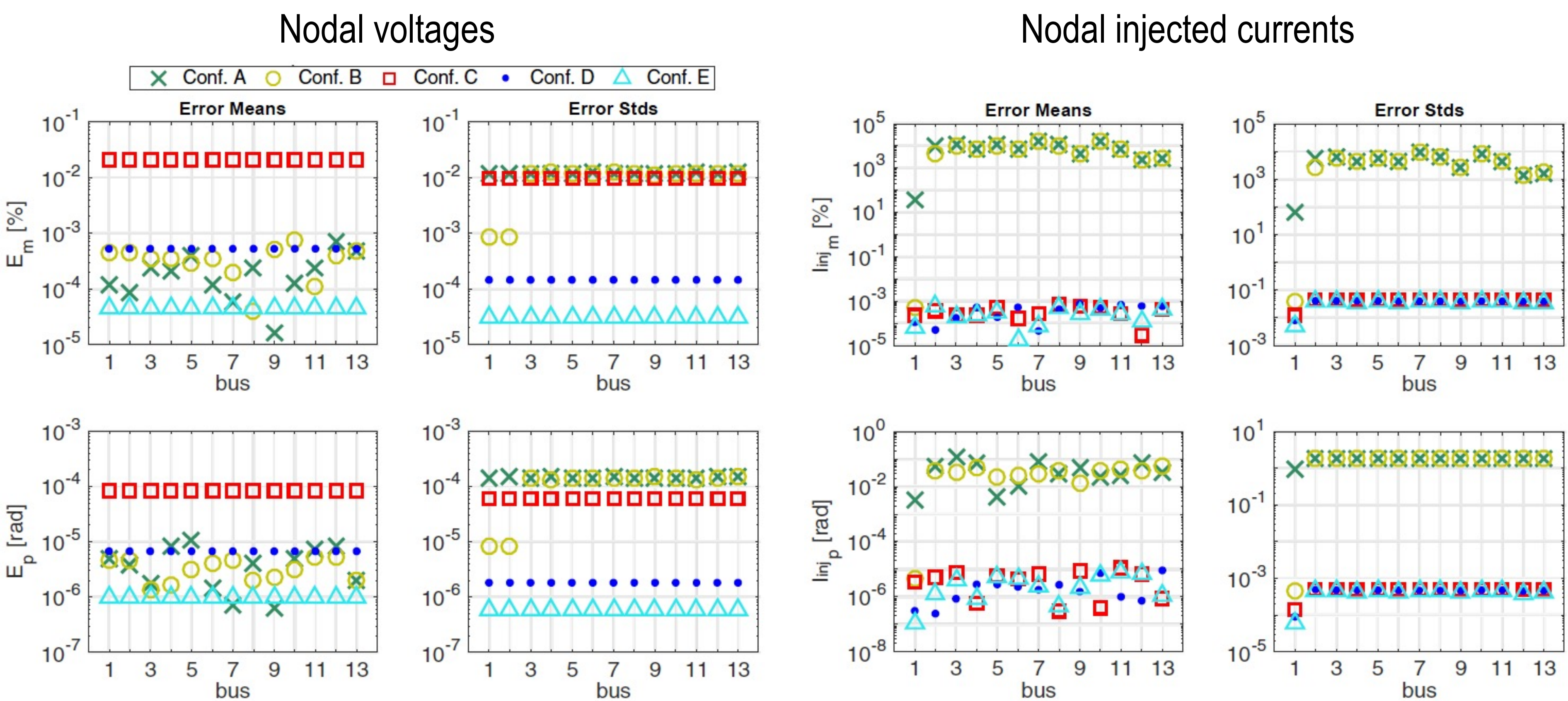

# Extension to complex distribution systems [3-5]

## Numerical results – Case 2 (high load scenario)

Means and stds of the estimation errors of magnitude/phase of voltages and injected currents for each measurement config (only the largest error among the three phases is shown).

Nodal voltages

Nodal injected currents

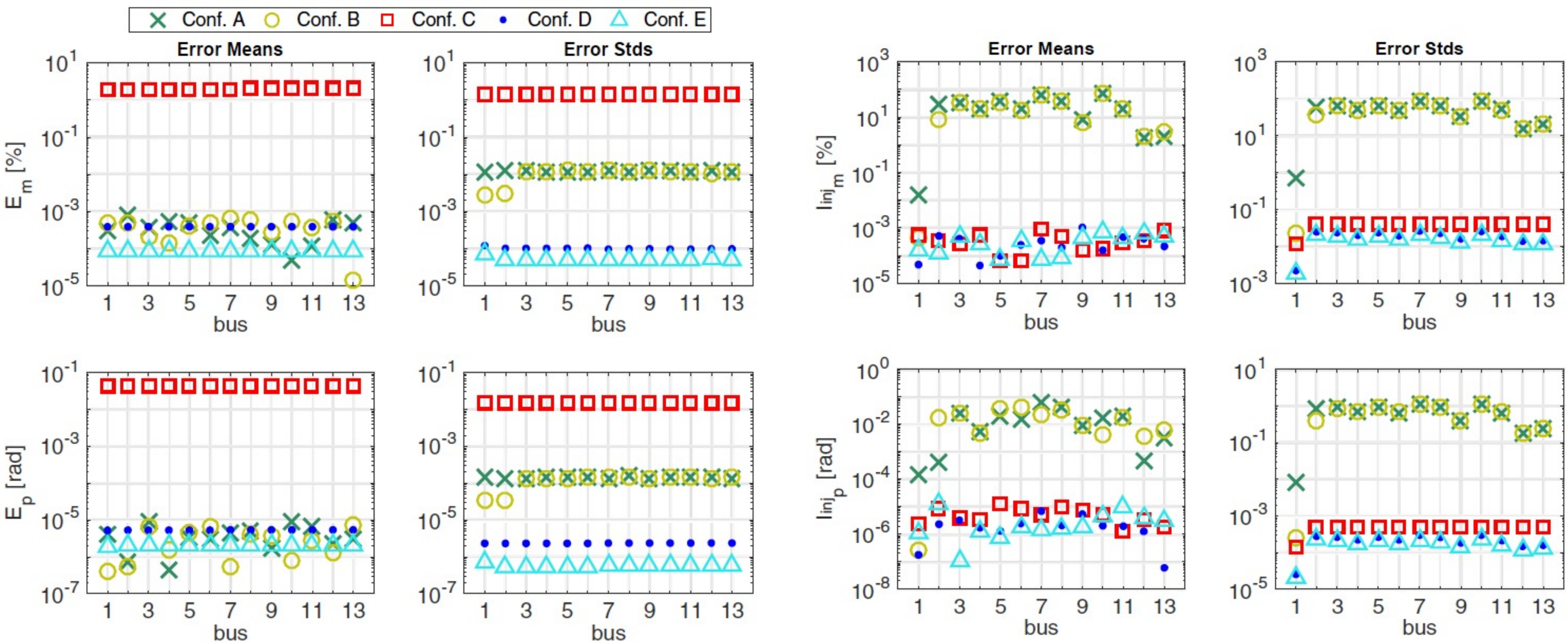

# Extension to complex distribution systems [3-5]

## Preliminary conclusions

- Measurement configurations composed of only voltages or only currents (*Conf. A* and *C*) are unable to provide accurate estimates in terms of currents and voltages, respectively. A better estimation accuracy is achieved by using mixed voltage and current measurements.

- *Conf. B*, consisting mainly on voltage measurements, leads to major errors on the current estimates, whilst *Conf. D*, composed mainly of current measurements, provides accurate voltage and current estimates.

- *Conf. E* improves only the voltage estimates compared to *Conf. D*.

- **Current measurements appears to be crucial for PMU-based linear state estimation in distribution systems**. This is due to the **specific characteristics and operational conditions of distribution systems resulting into reduced voltage magnitude variations and phase displacements that can be comparable with the uncertainties of the voltage phasor measurements.**

# Extension to complex distribution systems [3-5]

## Preliminary conclusions

- As a consequence, **measurement sets composed mainly of voltages (*Conf. A* and *B*) result in large errors of the current estimates**. For example, *Conf. A* **requires measurement uncertainties in the order of $10^{-6}$ % and $10^{-8}$ rad in order to get the same SE accuracy of** *Conf. D*. Note that **such a phase accuracy is well below the limit of currently available time synchronization systems**.

- *Conf. D* **allows obtaining accurate voltage and current estimates irrespectively of the network operating condition and with the minimum number of measurements**. The voltage and current estimation errors are always below 0.04 % in terms of magnitude and 0.5 mrad in terms of phase. **This accuracy is sufficient for a distribution system operator to exploit most of the functionalities that can be associated to a SE process, such as voltage control, line congestion management, optimal dispatch of DERs**.

# Fault Location and System Restoration (FLISR) using synchrophasor-based Real-Time State Estimation (RTSE)

# FLISR using synchrophasor-based RTSE

The importance of fault detection, fault location and quick power restoration is rapidly rising due to:

- Increasing number of faults as load density increases;
- More stringent requirements for SAIDI and SAIFI indexes to improve the quality of service;
- Increasing number of “plug and play” DERs that continuously change the short-circuit levels

*“ Current protection schemes are seen to be very rigid for the changing conditions in the network, so new adaptive solutions will be required in the future ”*

Cited from [*Protection of Distribution Systems with Distributed Energy Resources, Cigré-CIRED WG B5-C6.26 Final Report* ]

# FLISR using synchrophasor-based RTSE

## Method [6]

Normal operating conditions (no fault)

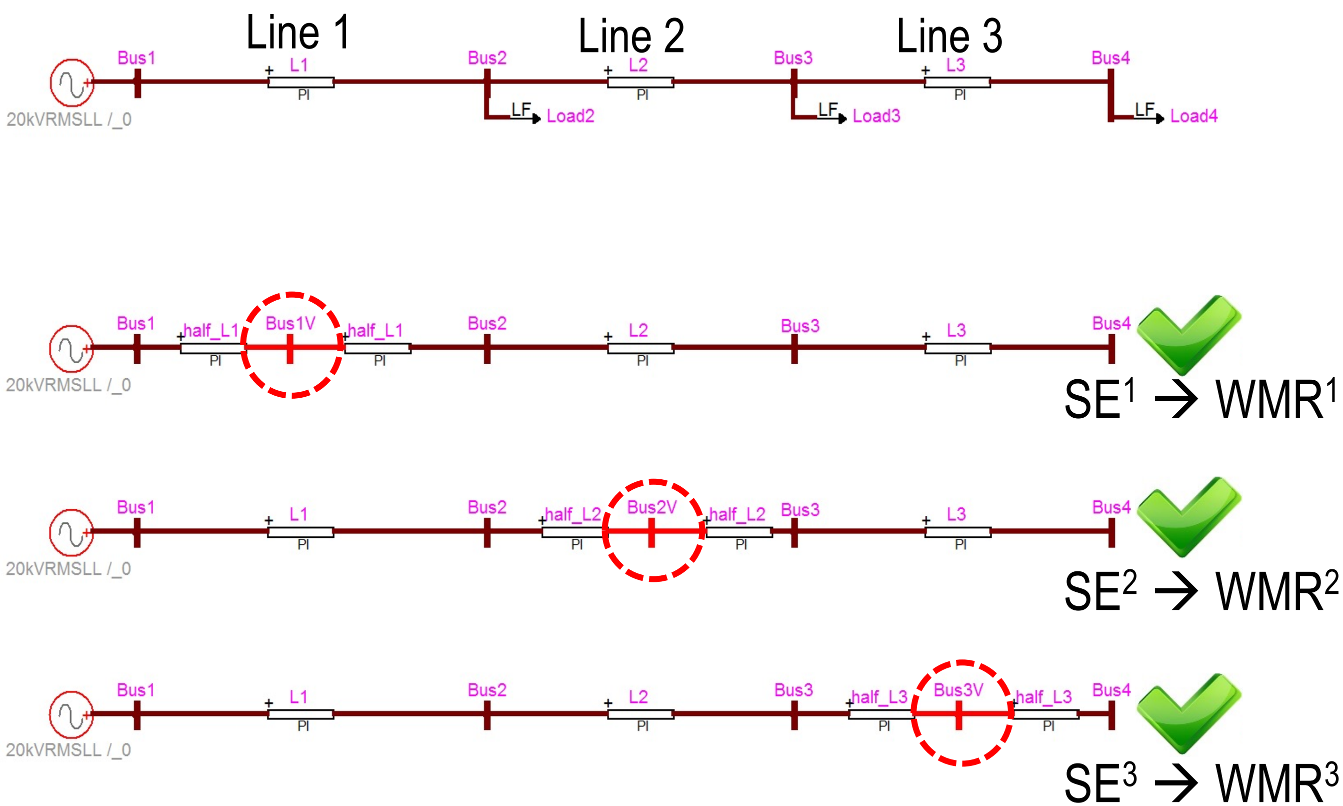


Metric: compare WMR for all SEs

$$\mathrm{WMR}^j = \sum_{i=1}^{m} \frac{\left| z_i - \hat{z}_i^{\,j} \right|}{\sigma_{z_i}}$$

All the SEs have a similar WMR

# FLISR using synchrophasor-based RTSE

## Method [6]

Normal operating conditions (no fault)

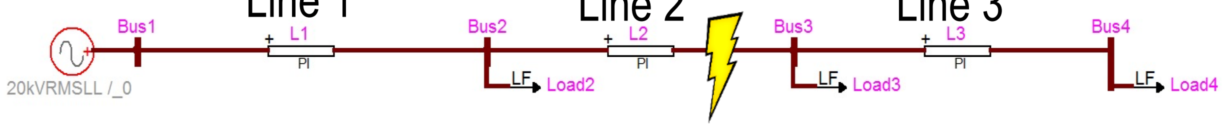


Additional bus in Line 2 (topology changes)

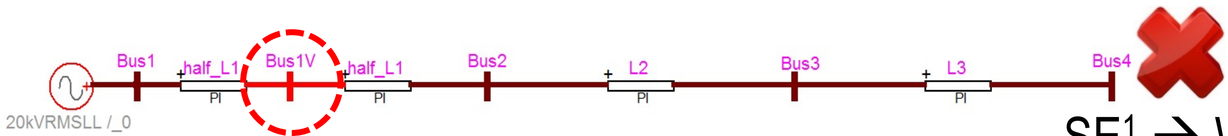


$SE^1 \rightarrow WMR^1$

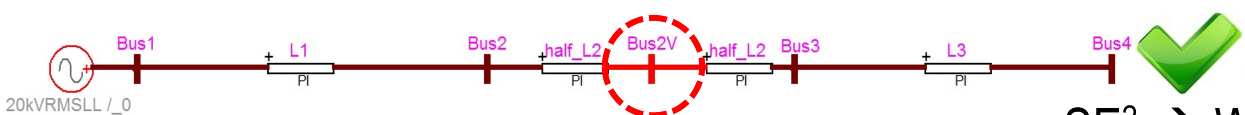


$SE^2 \rightarrow WMR^2$

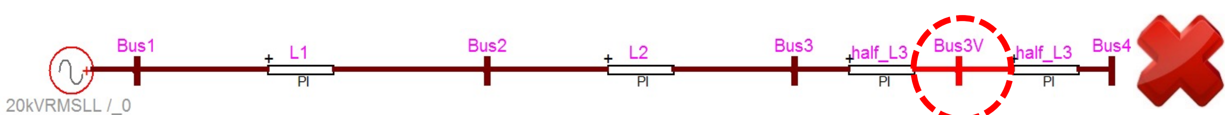


$SE^3 \rightarrow WMR^3$

Topology of $SE^2$

$\approx$

Real topology

$$\min(WMR^1, WMR^2, WMR^3) = \\ = WMR^2$$

Line 2 is faulted

# FLISR using synchrophasor-based RTSE

## Validation using a real-time simulator [6]

### MV feeder characteristics

- Location: Huissen, the Netherlands
- Size: 18 buses
- Nominal voltage: 10 kV (phase to phase)

### Real-time model includes:

- 3-phase unbalanced network
- Metrological model of PMUs (simulated) installed in every node measuring nodal voltages and currents injections/absorptions
- Metrological model of voltage and current sensors (including their uncertainty)

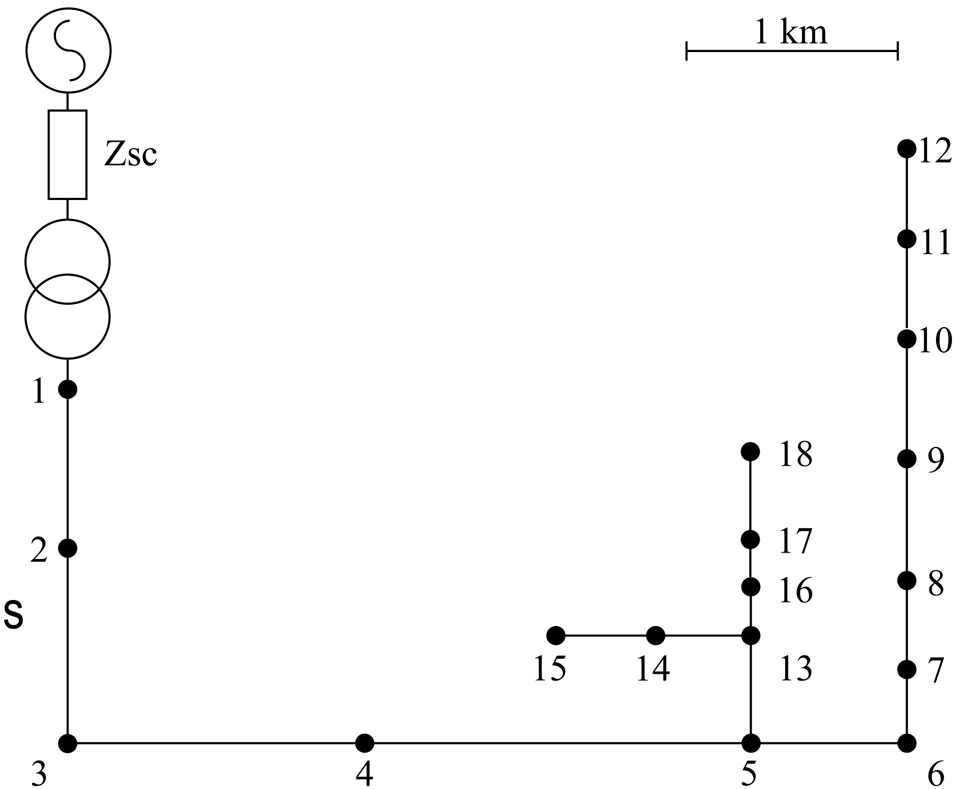

# FLISR using synchrophasor-based RTSE - Performances

## Validation via a real-time simulator [6]

TABLE I
3-PH FAULT, 1 Ω

| Fault Position | | Noise Level 1 | Noise Level 10 |
|---|---|---|---|
| $L_{4,5}$ | 1/4 | 100% | 100% |
| | 1/2 | 100% | 100% |
| $L_{9,10}$ | 1/4 | 100% | 100% |
| | 1/2 | 100% | 100% |
| $L_{13,16}$ | 1/4 | 100% | 100% |
| | 1/2 | 100% | 100% |

TABLE II
3-PH FAULT, 100 Ω

| Fault Position | | Noise Level 1 | Noise Level 10 |
|---|---|---|---|
| $L_{4,5}$ | 1/4 | 100% | 99.27% |
| | 1/2 | 100% | 99.85% |
| $L_{9,10}$ | 1/4 | 100% | 98.54% |
| | 1/2 | 100% | 99.90% |
| $L_{13,16}$ | 1/4 | 100% | 84.65% |
| | 1/2 | 100% | 99.74% |

TABLE III
2-PH FAULT: EARTHED NEUTRAL, 1 Ω

| Fault Position | | Noise Level 1 | Noise Level 10 |
|---|---|---|---|
| $L_{4,5}$ | 1/4 | 100% | 100% |
| | 1/2 | 100% | 100% |
| $L_{9,10}$ | 1/4 | 100% | 100% |
| | 1/2 | 100% | 100% |
| $L_{13,16}$ | 1/4 | 100% | 100% |
| | 1/2 | 100% | 100% |

TABLE IV
2-PH FAULT: EARTHED NEUTRAL, 100 Ω

| Fault Position | | Noise Level 1 | Noise Level 10 |
|---|---|---|---|
| $L_{4,5}$ | 1/4 | 100% | 92.48% |
| | 1/2 | 100% | 92.91% |
| $L_{9,10}$ | 1/4 | 100% | 89.56% |
| | 1/2 | 100% | 95.09% |
| $L_{13,16}$ | 1/4 | 100% | 68.43% |
| | 1/2 | 100% | 91.73% |

TABLE VII
1-PH-TO-GROUND FAULT: EARTHED NEUTRAL, 1 Ω

| Fault Position | | Noise Level 1 | Noise Level 10 |
|---|---|---|---|
| $L_{4,5}$ | 1/4 | 100% | 100% |
| | 1/2 | 100% | 100% |
| $L_{9,10}$ | 1/4 | 100% | 100% |
| | 1/2 | 100% | 100% |
| $L_{13,16}$ | 1/4 | 100% | 100% |
| | 1/2 | 100% | 100% |

TABLE VIII
1-PH-TO-GROUND FAULT: EARTHED NEUTRAL, 100 Ω

| Fault Position | | Noise Level 1 | Noise Level 10 |
|---|---|---|---|
| $L_{4,5}$ | 1/4 | 100% | 83.78% |
| | 1/2 | 100% | 99.99% |
| $L_{9,10}$ | 1/4 | 100% | 95.05% |
| | 1/2 | 100% | 99.23% |
| $L_{13,16}$ | 1/4 | 100% | 96.06% |
| | 1/2 | 100% | 99.36% |

TABLE IX
1-PH-TO GROUND FAULT: UNEARTHED NEUTRAL, 1 Ω

| Fault Position | | Noise Level 1 | Noise Level 10 |
|---|---|---|---|
| $L_{4,5}$ | 1/4 | 100% | 69.84% |
| | 1/2 | 100% | 87.28% |
| $L_{9,10}$ | 1/4 | 100% | 72.69% |
| | 1/2 | 100% | 77.82% |
| $L_{13,16}$ | 1/4 | 100% | 72.08% |
| | 1/2 | 100% | 79.33% |

TABLE X
1-PH-TO GROUND FAULT: UNEARTHED NEUTRAL, 100 Ω

| Fault Position | | Noise Level 1 | Noise Level 10 |
|---|---|---|---|
| $L_{4,5}$ | 1/4 | 100% | 70.95% |
| | 1/2 | 100% | 99.66% |
| $L_{9,10}$ | 1/4 | 100% | 89.99% |
| | 1/2 | 100% | 97.94% |
| $L_{13,16}$ | 1/4 | 100% | 87.56% |
| | 1/2 | 100% | 95.74% |

# FLISR using synchrophasor-based RTSE - Performances

## Latency assessment [6]

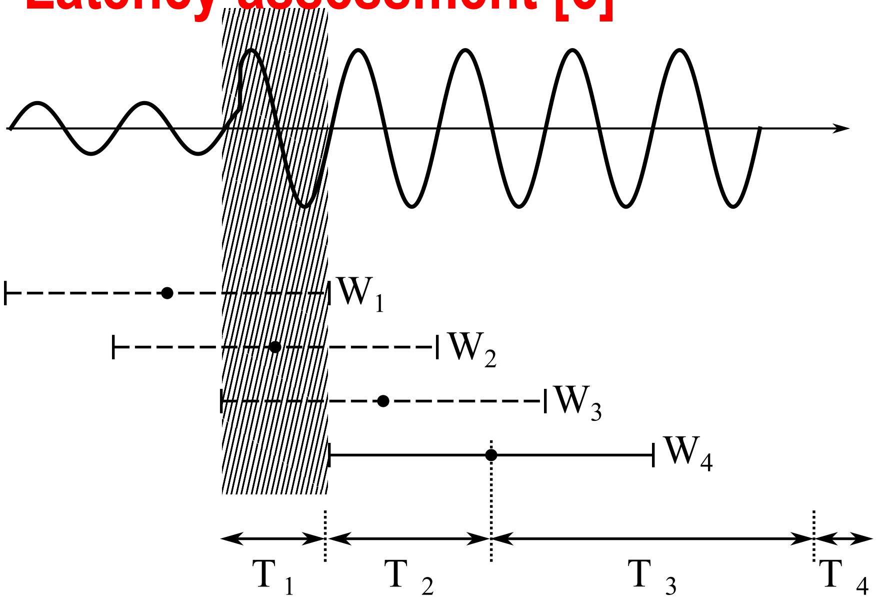


$T_1 = 0 \div 20$ ms $T_2 = 30$ ms $T_3 = 61$ ms $T_4 = 11$ ms

- **$T_1$**: depends on the fault position within the PMU observation window
- **$T_2$**: half of the PMU observation window
- **$T_3$**: synchrophasor data latency (assuming ideal network);
- **$T_4$**: computation time of the 17 state estimators

**Total latency: 78 ÷ 98 ms**

(without the

telecom network latency)

# On the joint class P+M synchrophasor estimation

# Synchrophasor Estimation Algorithms

## Window based Synchrophasor Estimation Algorithms

| Class | Typical algorithms | Advantages | Drawbacks |
|---|---|---|---|
| DFT based | Fourier analysis | Low computational complexity, harmonic rejection | Spectral leakage, Harmonic interference, Off-nominal freq. |
| | Interpolated DFT | | |
| Wavelet based | Recursive wavelet | Harmonic rejection | Computational complexity |
| Optimization based | WLS | They usually provide accurate estimates in combination with other methods | Non deterministic: driven by optimality criteria |
| | Kalman Filter | | |
| Taylor series based | Dynamic Phasor | It intrinsically reflects the dynamic behaviors of power systems | Computational complexity |

# DFT-based synchrophasor estimation

## Main sources of errors

1. Aliasing

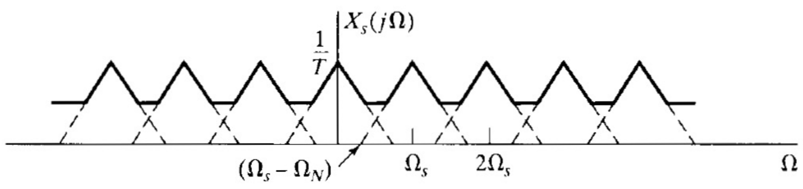


2. Long range leakage

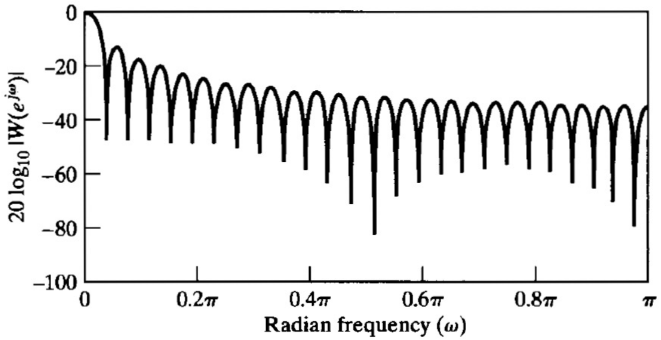


3. Short range leakage

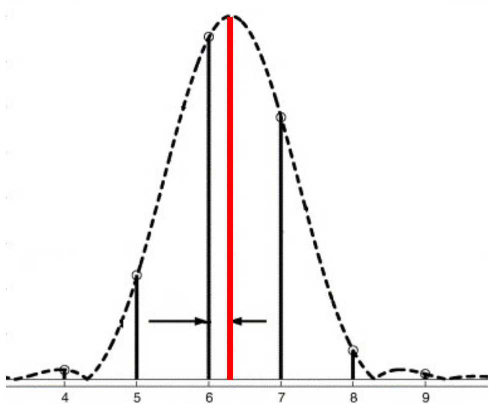


4. Harmonic interference

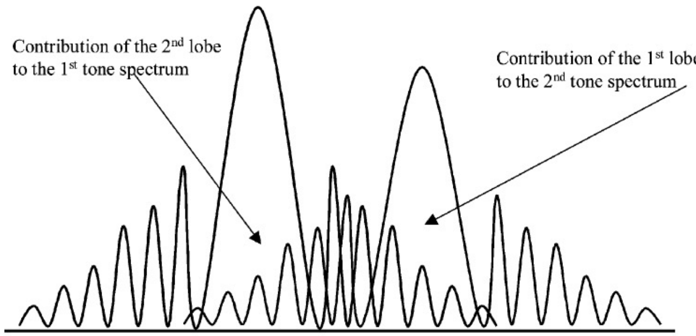

# DFT-based synchrophasor estimation

## Possible corrections

1. Aliasing

- Introduction of adequate anti-aliasing filters
- Increasing of the sampling frequency

2. Long range leakage

- Use of appropriate windowing functions

3. Short range leakage

- Interpolated DFT methods

4. Harmonic interference

- Iterative compensation of the self-interaction

# Joint P+M class synchrophasor estimation

## IpDFT problem solution for cos$^\alpha$ window functions [7]

The IpDFT is a technique to extract the parameters $f_0$, $A_0$ and $\varphi_0$ of a sinusoidal waveform by interpolating the highest DFT bins of the signal spectrum. It mitigates the effects of incoherent sampling ($f_0/\Delta f \notin \mathbb{N}$):

- Interpolating the highest DFT bins ➔ minimize spectral sampling

$$\delta = a \cdot \varepsilon \frac{|X(k_m+\varepsilon)| - |X(k_m-\varepsilon)|}{|X(k_m-\varepsilon)| + 2|X(k_m)| + |X(k_m+\varepsilon)|}, \quad a = 1.5 \text{ cos}, \; a = 2 \text{ hann}$$

$$f_0 = (k_m + \delta)\Delta f$$

$$\varphi_0 = \angle X(k_m) - \pi\delta$$

$$A_{0C} = 4 \cdot |X(k_m)| \left| \frac{\delta^2 - 0.25}{\cos(\pi\delta)} \right|$$

$$A_{0H} = |X(k_m)| \left| \frac{\pi\delta}{\sin(\pi\delta)} \right| |\delta^2 - 1|$$

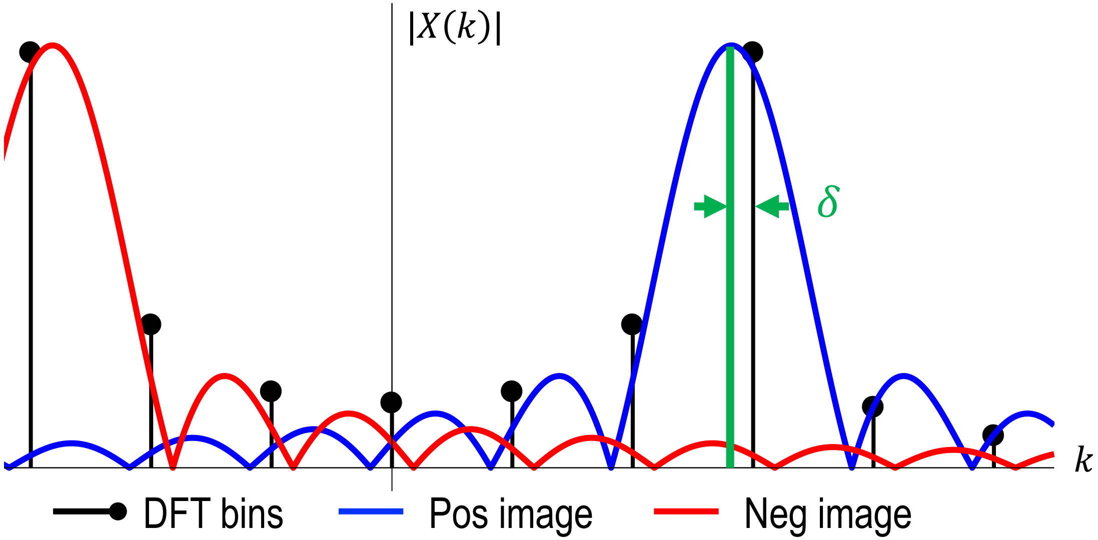

# Joint P+M class synchrophasor estimation

## Enhanced-IpDFT algorithm [7]

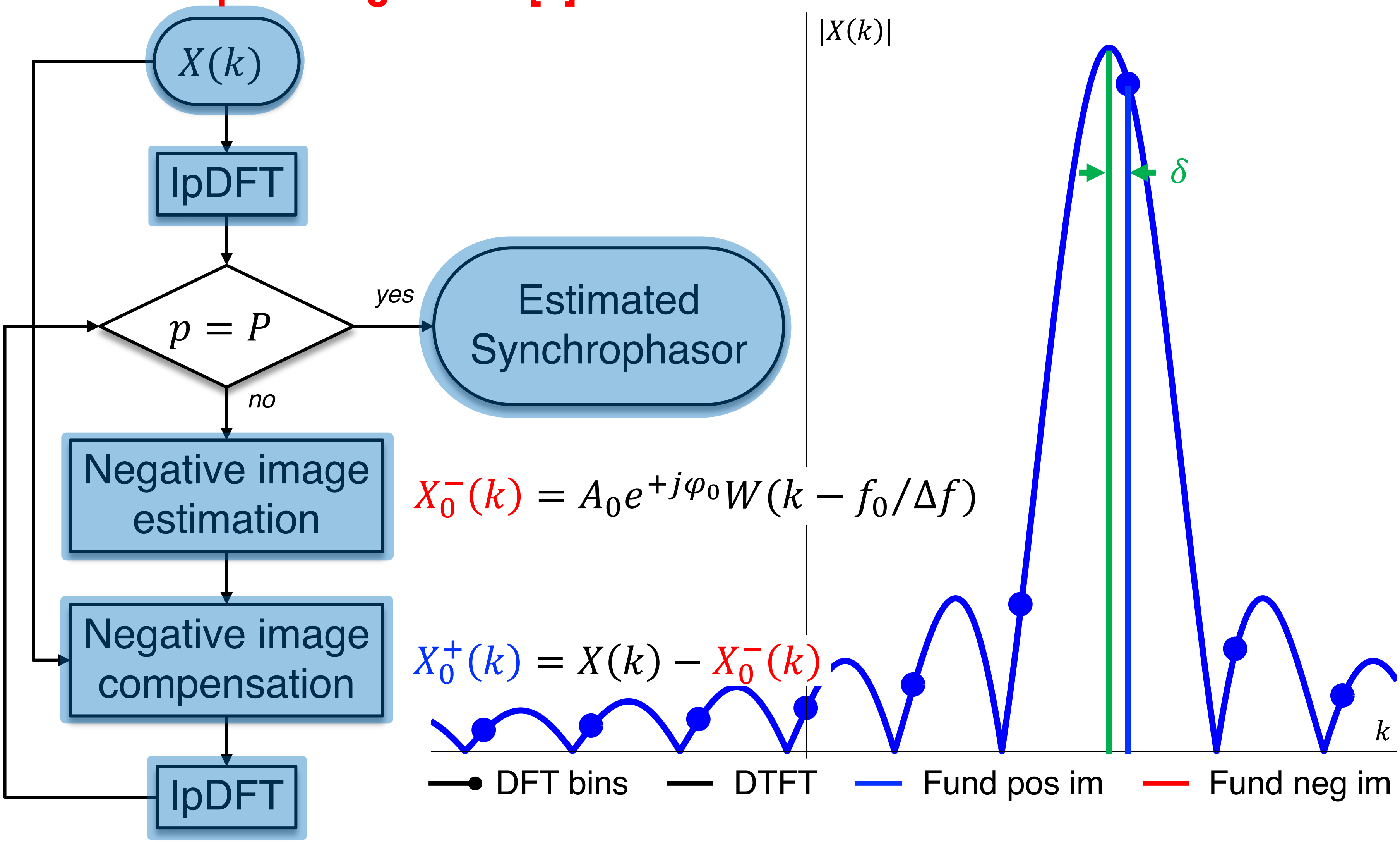


$$X_0^-(k) = A_0 e^{+j\varphi_0} W(k - f_0/\Delta f)$$

$$X_0^+(k) = X(k) - X_0^-(k)$$

# Joint P+M class synchrophasor estimation

## Enhanced-IpDFT algorithm: poor performance against OOBI

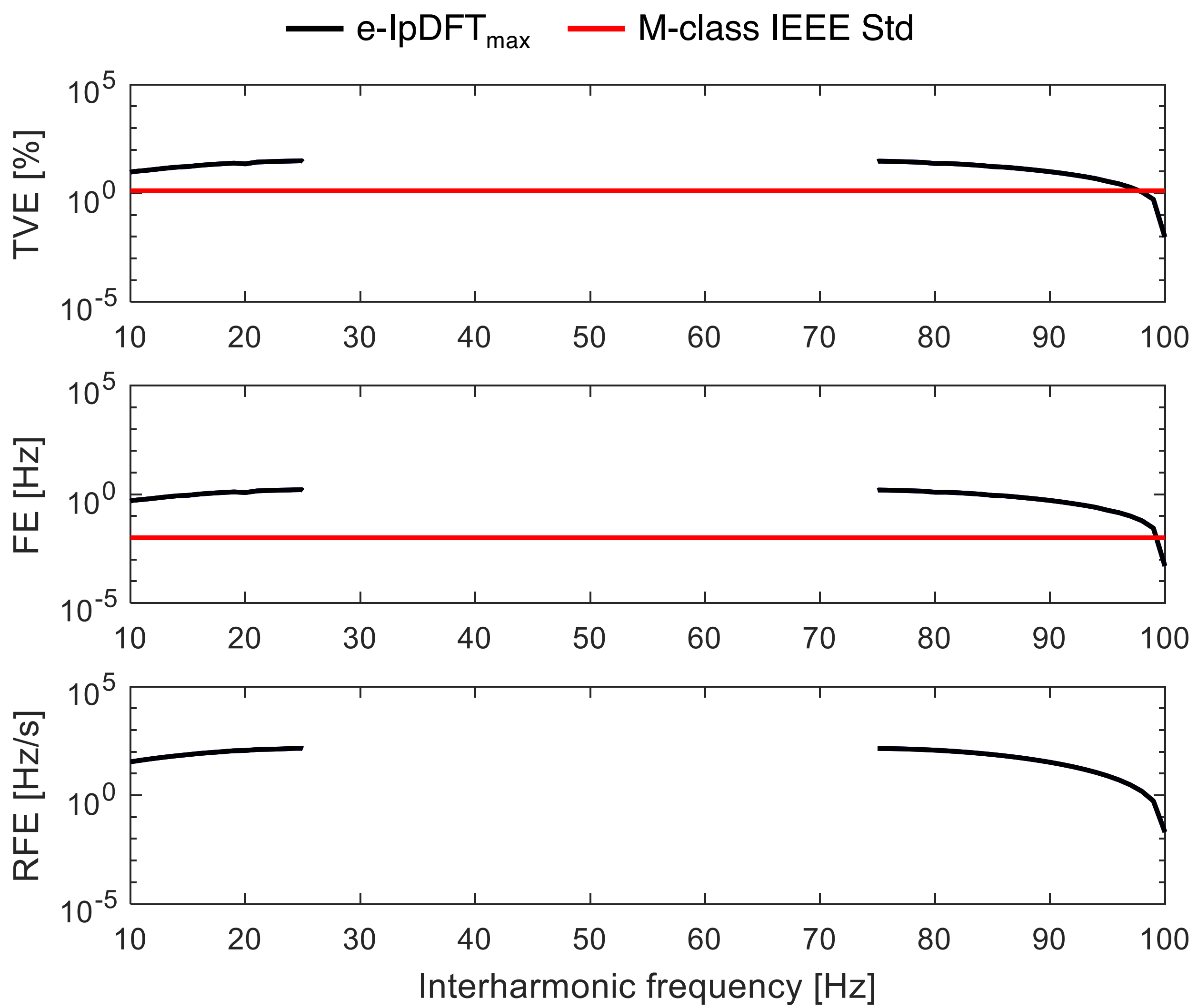


**Max Errors:**

**TVE**
IEEE Std = 1.3%
e-IpDFT = 31%

**FE**
IEEE Std = 10 mHz
e-IpDFT = 1.6 Hz

**RFE**
e-IpDFT = 145 Hz/s

# Joint P+M class synchrophasor estimation

## Iterative-IpDFT algorithm [8]

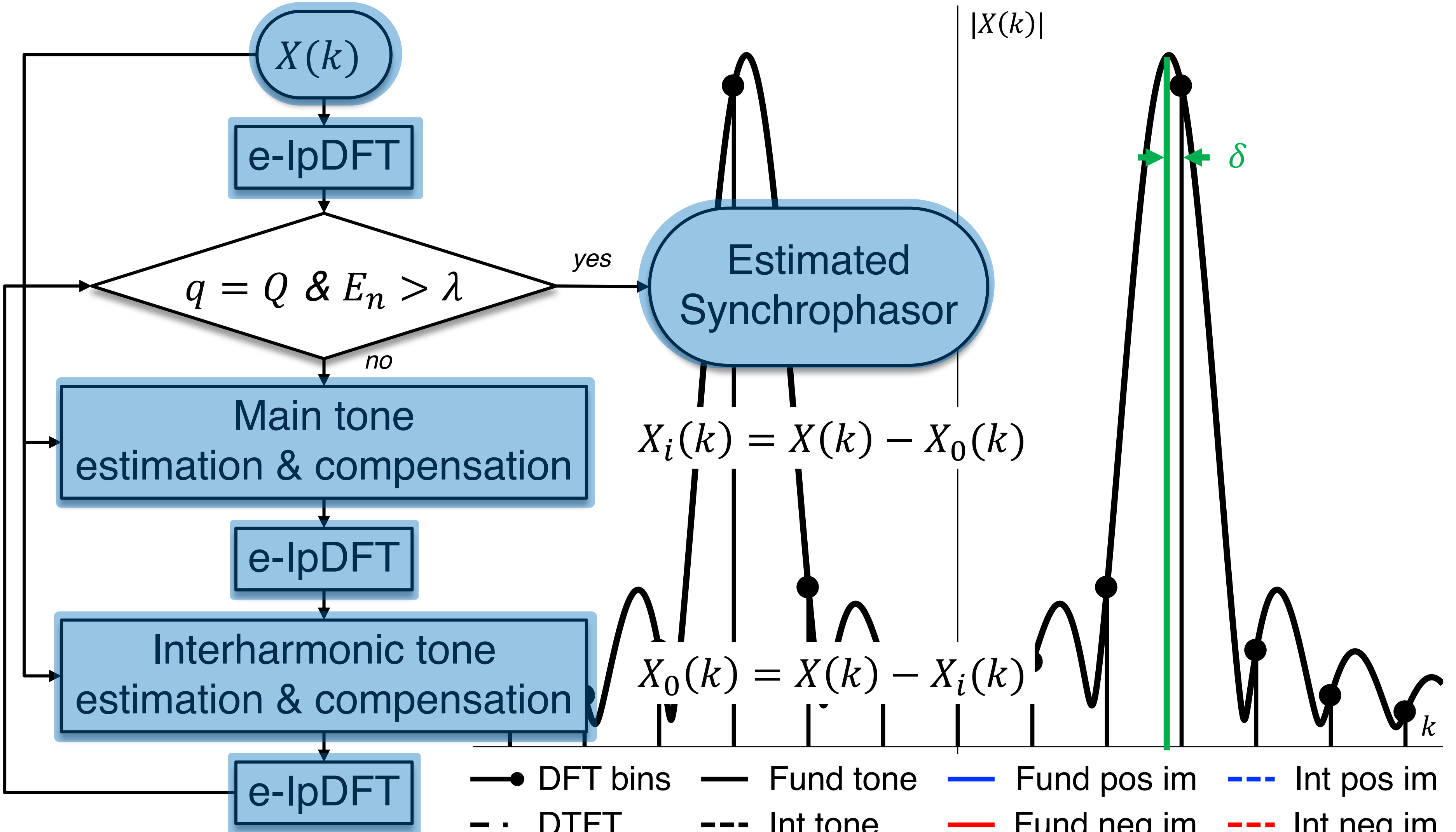

# Joint P+M class synchrophasor estimation

## Iterative-IpDFT algorithm performance and P+M compliance [8]
## Static conditions

| | TVE [%] | | | | | | FE [mHz] | | | | | | RFE [Hz/s] | | | | | |
|---|---|---|---|---|---|---|---|---|---|---|---|---|---|---|---|---|---|---|
| | IEEE Std | | i-IpDFT | | | | IEEE Std | | i-IpDFT | | | | IEEE Std | | i-IpDFT | | | |
| | P | M | cos SNR [dB] | | Hann SNR [dB] | | P | M | cos SNR [dB] | | Hann SNR [dB] | | P | M | cos SNR [dB] | | Hann SNR [dB] | |
| | | | 60 | 80 | 60 | 80 | | | 60 | 80 | 60 | 80 | | | 60 | 80 | 60 | 80 |
| Sign Freq | 1 | 1 | 0.024 | 0.002 | 0.03 | 0.003 | 5 | 5 | 1.3 | 0.1 | 1.5 | 0.1 | 0.4 | 0.1 | 0.095 | 0.009 | 0.126 | 0.012 |
| Harm Dist 1% | 1 | 1 | 0.108 | 0.094 | 0.028 | 0.003 | 5 | 25 | 5.4 | 4.7 | 1.3 | 0.1 | 0.4 | - | 0.086 | 0.009 | 0.112 | 0.011 |
| Harm Dist 10% | 1 | 1 | 0.055 | 0.047 | 0.026 | 0.003 | 5 | 25 | 2 | 1.1 | 1.2 | 0.1 | 0.4 | - | 0.085 | 0.009 | 0.124 | 0.011 |
| OOBI $f_0$=47.5 Hz | - | 1.3 | 0.056 | 0.022 | 0.108 | 0.082 | - | 10 | 2.7 | 1.1 | 5.6 | 4.1 | - | - | 0.217 | 0.101 | 0.513 | 0.369 |
| OOBI $f_0$=50 Hz | - | 1.3 | 0.026 | 0.003 | 0.033 | 0.004 | - | 10 | 1.3 | 0.1 | 1.7 | 0.2 | - | - | 0.104 | 0.009 | 0.153 | 0.013 |
| OOBI $f_0$=52.5 Hz | - | 1.3 | 0.043 | 0.004 | 0.044 | 0.011 | - | 10 | 2.1 | 0.2 | 2.2 | 0.6 | - | - | 0.143 | 0.022 | 0.150 | 0.032 |

# Joint P+M class synchrophasor estimation

## Iterative-IpDFT algorithm performance and P+M compliance [8]
## Dynamic conditions

| | TVE [%] | | | | | | FE [mHz] | | | | | | RFE [Hz/s] | | | | | |
|---|---|---|---|---|---|---|---|---|---|---|---|---|---|---|---|---|---|---|
| | IEEE Std | | i-IpDFT | | | | IEEE Std | | i-IpDFT | | | | IEEE Std | | i-IpDFT | | | |
| | P | M | cos | | Hann | | P | M | cos | | Hann | | P | M | cos | | Hann | |
| | | | SNR [dB] | | SNR [dB] | | | | SNR [dB] | | SNR [dB] | | | | SNR [dB] | | SNR [dB] | |
| | | | 60 | 80 | 60 | 80 | | | 60 | 80 | 60 | 80 | | | 60 | 80 | 60 | 80 |
| Ampl Mod | 3 | 3 | 0.846 | 0.847 | 0.604 | 0.604 | 60 | 300 | 2.2 | 1.6 | 1.6 | 0.4 | 2.3 | 14 | 0.106 | 0.051 | 0.123 | 0.016 |
| Ph Mod | 3 | 3 | 0.805 | 0.806 | 0.547 | 0.547 | 60 | 300 | 21.9 | 22 | 17.9 | 17.4 | 2.3 | 14 | 0.725 | 0.683 | 0.568 | 0.540 |
| Freq Ramp | 1 | 1 | 0.058 | 0.055 | 0.044 | 0.038 | 10 | 10 | 1 | 0.2 | 0.9 | 0.2 | 0.4 | 0.2 | 0.088 | 0.011 | 0.083 | 0.011 |

| | TVE Response time [s] | | | | | | FE Response time [s] | | | | | | RFE Response time [s] | | | | | |
|---|---|---|---|---|---|---|---|---|---|---|---|---|---|---|---|---|---|---|
| | IEEE Std | | i-IpDFT | | | | IEEE Std | | i-IpDFT | | | | IEEE Std | | i-IpDFT | | | |
| | P | M | cos | | Hann | | P | M | cos | | Hann | | P | M | cos | | Hann | |
| | | | SNR [dB] | | SNR [dB] | | | | SNR [dB] | | SNR [dB] | | | | SNR [dB] | | SNR [dB] | |
| | | | 60 | 80 | 60 | 80 | | | 60 | 80 | 60 | 80 | | | 60 | 80 | 60 | 80 |
| Ampl Step | 0.04 | 0.14 | 0.034 | 0.034 | 0.028 | 0.028 | 0.09 | 0.28 | 0.048 | 0.048 | 0.044 | 0.044 | 0.12 | 0.28 | 0.056 | 0.056 | 0.054 | 0.054 |
| Ph Step | 0.04 | 0.14 | 0.040 | 0.040 | 0.032 | 0.032 | 0.09 | 0.28 | 0.048 | 0.048 | 0.044 | 0.044 | 0.12 | 0.28 | 0.054 | 0.054 | 0.054 | 0.054 |

| | Delay time [s] | | | | | | Max Overshoot [%] | | | | | |
|---|---|---|---|---|---|---|---|---|---|---|---|---|
| | IEEE Std | | i-IpDFT | | | | IEEE Std | | i-IpDFT | | | |
| | P | M | cos | | Hann | | P | M | cos | | Hann | |
| | | | SNR [dB] | | SNR [dB] | | | | SNR [dB] | | SNR [dB] | |
| | | | 60 | 80 | 60 | 80 | | | 60 | 80 | 60 | 80 |
| Ampl Step | 0.005 | 0.005 | 0.002 | 0.002 | 0.002 | 0.002 | 5 | 10 | 0 | 0 | 0 | 0 |
| Ph Step | 0.005 | 0.005 | 0.002 | 0.002 | 0.002 | 0.002 | 5 | 10 | 0 | 0 | 0 | 0 |

# Conclusions

# Conclusions

- Future control and protection applications for power distribution networks are expected to make large use of PMUs.
- PMU-based state estimation of power distribution networks should rely more on current measurements in order to not require extremely low accuracy levels on voltage synchrophasor measurements.
- In order to minimize the duplication of devices, synchrophasor estimators be compliant with both P+M classes.
- Example of applications that can directly benefit from these characteristics are:
    - real-time situational awareness used by grid-aware control applications (i.e., OPF-based);
    - PMU-based protection and fault location potentially replacing traditional schemes.

# References


1. Cigre WG B5.14, "Wide area protection and control technologies," tech. rep., September 2016 https://e-cigre.org/publication/664-wide-area-protection--control-technologies
2. D. Novosel, V. Madani, B. Bhargave, K. Vu, and J. Cole, "Dawn of the grid synchronization," IEEE Power and Energy Magazine, vol. 6, pp. 49-60, January 2008.
3. L. Zanni, D. Colangelo, R. Cherkaoui and M. Paolone, "Impact of Synchrophasor Measurement Types and Uncertainties on the Accuracy of Distribution System Linear State Estimators," Proceedings of the 2015 IEEE PES PowerTech, Eindhoven, The Netherlands, June 29 - July 2, 2015.
4. A. Abur and A. Expo´sito, Power System State Estimation: Theory and Implementation, ser. Power Engineering (Willis). Taylor & Francis, 2004.
5. M. Paolone et al., chapter "Static and recursive PMU-based State Estimation Processes for transmission and distribution grids", in the book "Advanced Techniques for Power System Modelling, Control and Stability Analysis", IET 2015.
6. M. Pignati, L. Zanni, P. Romano, R. Cherkaoui and M. Paolone, "Fault Detection and Faulted Line Identification in Active Distribution Networks Using Synchrophasors-based Real-Time State Estimation" IEEE Trans. on Power Delivery, vol. 32, no. 1, pp: 381– 392, Feb. 2017.
7. P. Romano and M. Paolone, "Enhanced interpolated-DFT for synchrophasor estimation in FPGAs: Theory, implementation, and validation of a PMU prototype," IEEE Transactions on Instrumentation and Measurement, vol. 63, no. 12, pp. 2824–2836, Dec 2014.

# References


8. A. Derviškadić, P. Romano and M. Paolone, “Iterative-Interpolated DFT for Synchrophasor Estimation: a Single Algorithm for P and M-class compliant PMUs”, IEEE Trans. on Instrumentation and Measurements, vol. 67, no. 3, pp. 547 - 558, March 2018
9. L. Zanni; J. Y. Le Boudec; R. Cherkaoui; M. Paolone, "A Prediction-Error Covariance Estimator for Adaptive Kalman Filtering in Step-Varying Processes: Application to Power-System State Estimation," in IEEE Transactions on Control Systems Technology, 2017.
10. M. Pignati, M. Popovic, S. Barreto, R. Cherkaoui, G. Dario Flores, J.-Y. Le Boudec, M. Mohiuddin, M. Paolone, P. Romano, S. Sarri, T. Tesfay, D.-C. Tomozei, L. Zanni, “Real-time state estimation of the EPFL-campus medium-voltage grid by using PMUs,” Proc. of the Innovative Smart Grid Technologies Conference (ISGT), 2015 IEEE Power & Energy Society, pp.1-5, 18-20 Feb. 2015, Washington DC, USA.

# Backup-slides

# Adaptive KF: estimation of the process model covariance from observations [9]

## Brief recap on standard KF theory

**Measurement model:**

measurement noise vector

measurements noise covariance matrix

$$\mathbf{z}_k = \mathbf{H}\,\mathbf{x}_k + \mathbf{v}_k \qquad p(\mathbf{v}_k) \sim N(0, \mathbf{R}_k)$$

**Process model:**

State-transition matrix

controllable inputs vector

process noise vector

process noise covariance matrix

$$\mathbf{x}_k = \mathbf{A}_k \mathbf{x}_{k-1} + \mathbf{B}_k \mathbf{u}_k + \mathbf{w}_k \qquad p(\mathbf{w}_k) \sim N(0, \mathbf{Q}_k)$$

**Historical challenges:**

- Process model should match the power-system state dynamics;
- **Robust computation of the process noise covariance matrix**;
- Complementary applications become more complicated (e.g., bad-data processing);
- Higher computational time.

# Adaptive KF: estimation of the process model covariance from observations [9]

*Prediction step*

$$\widehat{\mathbf{x}}_{k|k-1} = \widehat{\mathbf{x}}_{k-1|k-1}$$

$$\mathbf{P}_{k|k-1} = \mathbf{P}_{k-1|k-1} + \mathbf{Q}_k$$

$$\mathbf{y}_k = \mathbf{z}_k - \mathbf{H}\widehat{\mathbf{x}}_{k|k-1}$$

$$\boxed{\mathbf{T}_k = \mathbf{H}\mathbf{P}_{k|k-1}\mathbf{H}^T + \mathbf{R}_k}$$

$\widehat{\mathbf{C}}_k$ sample covariance from $N$ past innovations

*Estimation step*

$$\mathbf{L}_k = \mathbf{P}_{k|k-1}\mathbf{H}^T(\mathbf{H}\mathbf{P}_{k|k-1}\mathbf{H}^T + \mathbf{R}_k)^{-1}$$

$$\widehat{\mathbf{x}}_{k|k} = \widehat{\mathbf{x}}_{k|k-1} + \mathbf{L}_k(\mathbf{z}_k - \mathbf{H}\widehat{\mathbf{x}}_{k|k-1})$$

$$\mathbf{P}_{k|k} = (\mathbf{I} - \mathbf{L}_k\mathbf{H})\mathbf{P}_{k|k-1}$$

# Adaptive KF: estimation of the process model covariance from observations [9]

Maximum likelihood estimation of covariance matrix from the samples (constrained convex optimization problem)

$$\min_{\boldsymbol{\Sigma}} \quad \left\{ -\log\left[\det(\boldsymbol{\Sigma})\right] + \mathrm{trace}(\boldsymbol{\Sigma}\mathbf{E}) \right\}$$

$$\text{subject to:} \quad \boldsymbol{\Sigma} \text{ real symmetric and } \boldsymbol{\Sigma} \succ \mathbf{0}$$

$$\mathbf{I}_n - \boldsymbol{\Sigma} \succeq \mathbf{0}.$$

$$\widehat{\mathbf{P}}_{k|k-1} = \mathbf{U}^{-1}\left(\widehat{\boldsymbol{\Sigma}}^{-1} - \mathbf{I}_n\right)\mathbf{U}^{-T}$$

# Adaptive KF: estimation of the process model covariance from observations [9]

## EPFL 20kV dist. feeder (hosting 1MW BESS and 0.1 MW of PV, max load 0.3 MW) [10]

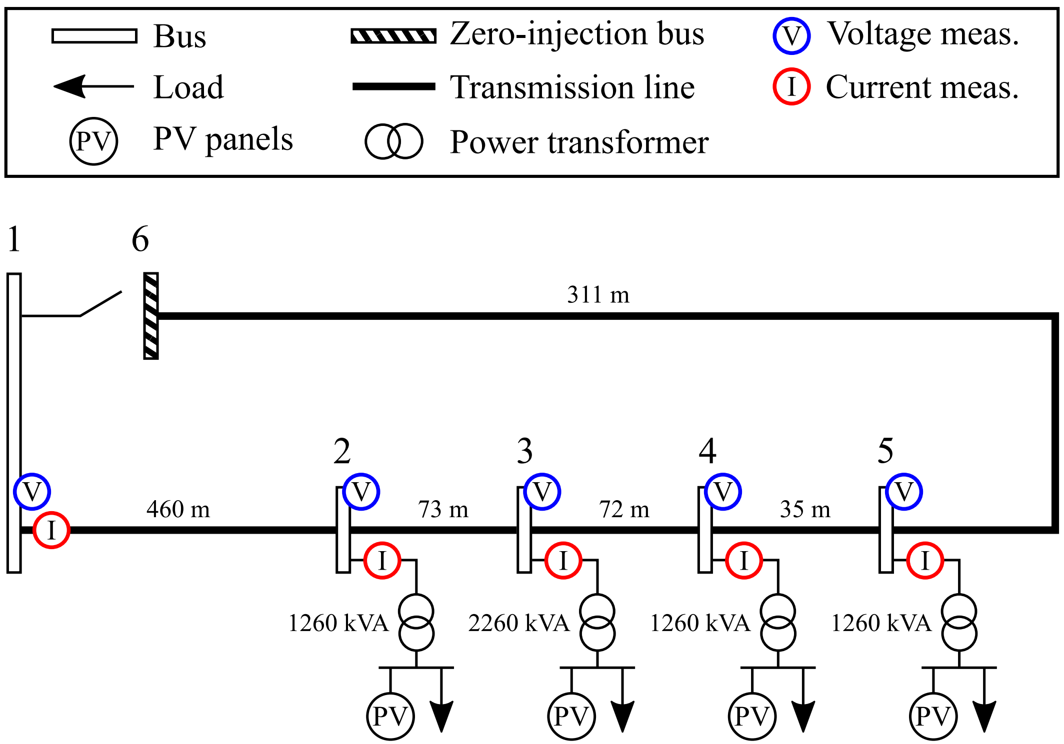


| | |
|---|---|
| Rated voltage | 20 kV |
| Voltage sensors | Capacitive 0.1-class |
| Current sensors | Rogowsky 0.5-class |

| | |
|---|---|
| Voltages | 3 x 5 |
| Current injections | 3 x 5 |
| Zero-inj. buses | 1 |
| Measurements | 66 |
| State variables | 36 |
| Redundancy | 1.8 |

# Adaptive KF: estimation of the process model covariance from observations [9]

## EPFL 20kV dist. feeder (hosting 1MW BESS and 0.1 MW of PV, max load 0.3 MW) [10]

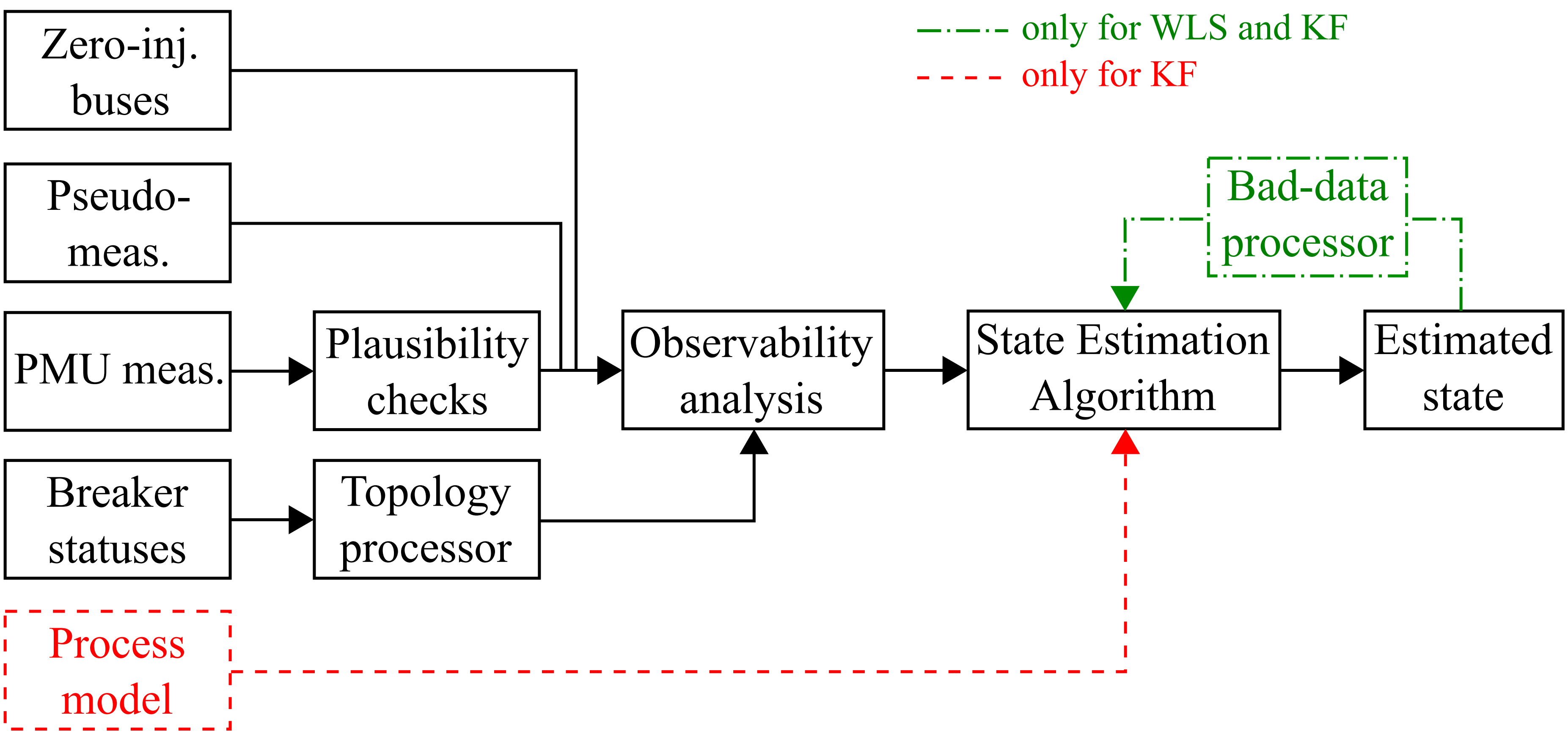

# Adaptive KF: estimation of the process model covariance from observations [9]

## EPFL 20kV dist. feeder (hosting 1MW BESS and 0.1 MW of PV, max load 0.3 MW) [10]